Efficient Nonthermal Particle Acceleration by the Kink Instability in Relativistic Jets

E. P. Alves, J. Zrake, and F. Fiuza

Phys. Rev. Lett. **121**, 245101 — Published 14 December 2018

DOI: 10.1103/PhysRevLett.121.245101

Efficient Nonthermal Particle Acceleration by the Kink Instability in Relativistic Jets

E. P. Alves,[1,*] J. Zrake,[2] and F. Fiuza[1,†]

[1] *High Energy Density Science Division, SLAC National Accelerator Laboratory, Menlo Park, CA 94025, USA*
[2] *Physics Department and Columbia Astrophysics Laboratory, Columbia University, 538 West 120th Street, New York, NY 10027*

Relativistic magnetized jets from active galaxies are among the most powerful cosmic accelerators, but their particle acceleration mechanisms remain a mystery. We present a new acceleration mechanism associated with the development of the helical kink instability in relativistic jets, which leads to the efficient conversion of the jet's magnetic energy into nonthermal particles. Large-scale three-dimensional *ab initio* simulations reveal that the formation of highly tangled magnetic fields and a large-scale inductive electric field throughout the kink-unstable region promotes rapid energization of the particles. The energy distribution of the accelerated particles develops a well-defined power-law tail extending to the radiation-reaction limited energy in the case of leptons, and to the confinement energy of the jet in the case of ions. When applied to the conditions of well-studied bright knots in jets from active galaxies, this mechanism can account for the spectrum of synchrotron and inverse Compton radiating particles, and offers a viable means of accelerating ultra-high-energy cosmic rays to 10^{20} eV.

Extragalactic radio jets are powerful outflows of relativistic magnetized plasma emanating from the central regions of active galaxies. These systems (known as active galactic nuclei, or AGNs) are among the most powerful accelerators of charged particles in the cosmos. They contain relativistic electrons and positrons which radiate, via synchrotron and inverse Compton processes, from radio waves to TeV γ-rays, attaining energies vastly in excess of the thermal mean [1]. AGN jets are also candidate sources of ultra-high-energy cosmic rays (UHECRs), whose energies are observed by ground-based detectors to exceed 10^{20} eV [2, 3]. This hypothesis has gained further support with the recent coincident detection of γ-rays and a high-energy neutrino from blazar TXS 0506+056 [4], which confirms that AGN jets accelerate high-energy cosmic rays.

The specific mechanisms by which relativistic jets accelerate charged particles to such high energies remains a long-standing mystery. Observations of bright knots in AGN jets (*e.g.* the well-studied HST-1 in M87) suggest that efficient particle acceleration may be taking place at distances of 10 pc to 1 kpc from the black hole central engine. At these distances the jet's energy exists primarily in the form of magnetic fields, observed to possess a tightly wound helical structure [5]. The bright knots are nearly stationary features, and are commonly interpreted as recollimation shocks associated with the interaction of the jet with the ambient medium [6, 7]. Historically, particle energization in these regions has been attributed to diffusive shock acceleration [8, 9]. However, recent work [10, 11] indicates that shock acceleration is not efficient in relativistic magnetically dominated plasma.

Another possibility is that particles accelerate by feeding on the copious free energy of the jet's internal magnetic field. This energy may be extracted via the development of hydromagnetic instabilities that act on the jet's helical magnetic field structure, the most relevant of which is thought to be the helical kink instability (KI) [12, 13]. Recent global magnetohydrodynamic (MHD) simulations of the launching and propagation of relativistic jets [14–16] confirm that the KI can indeed be triggered where the jet recollimates, playing an important role in the dissipation of the jet's magnetic energy. They also reveal that the KI operates internally, distorting only the spine of the jet, without disrupting its global morphology or its ability to propagate to larger distances [15, 17]. This is consistent with observations, which indicate that AGN jets remain globally stable over these bright recollimation regions [5, 6]. It remains unknown, however, *if* and *how* the magnetic energy dissipated by the internal KI is channeled into energetic nonthermal particles. This inherently kinetic physics is not captured within the framework of MHD.

In this Letter, we present the results of three-dimensional (3D), particle-in-cell (PIC) simulations that reveal for the first time how the self-consistent development of the internal KI in relativistic magnetized jets results in the efficient acceleration of nonthermal particles. We find that the emergence of highly tangled magnetic fields and a large-scale electric field throughout the kink-unstable region promotes rapid energization of the particles up to the confinement energy of the jet. Acceleration occurs over 10 light-crossing times of the jet cross-sectional radius, during which $\sim$50% of the jet's toroidal magnetic field energy is transfered to newly accelerated particles with a power-law spectrum. Importantly, we observe that the maximum energy gain increases linearly with the jet cross-sectional radius. Based on these findings, we argue that this new mechanism can account for the acceleration of high-energy leptons and hadrons in AGN jets.

We simulated a volume of the jet in its proper reference frame, with relativistic electron-positron plasma supporting a helical magnetic field in an unstable hydromagnetic

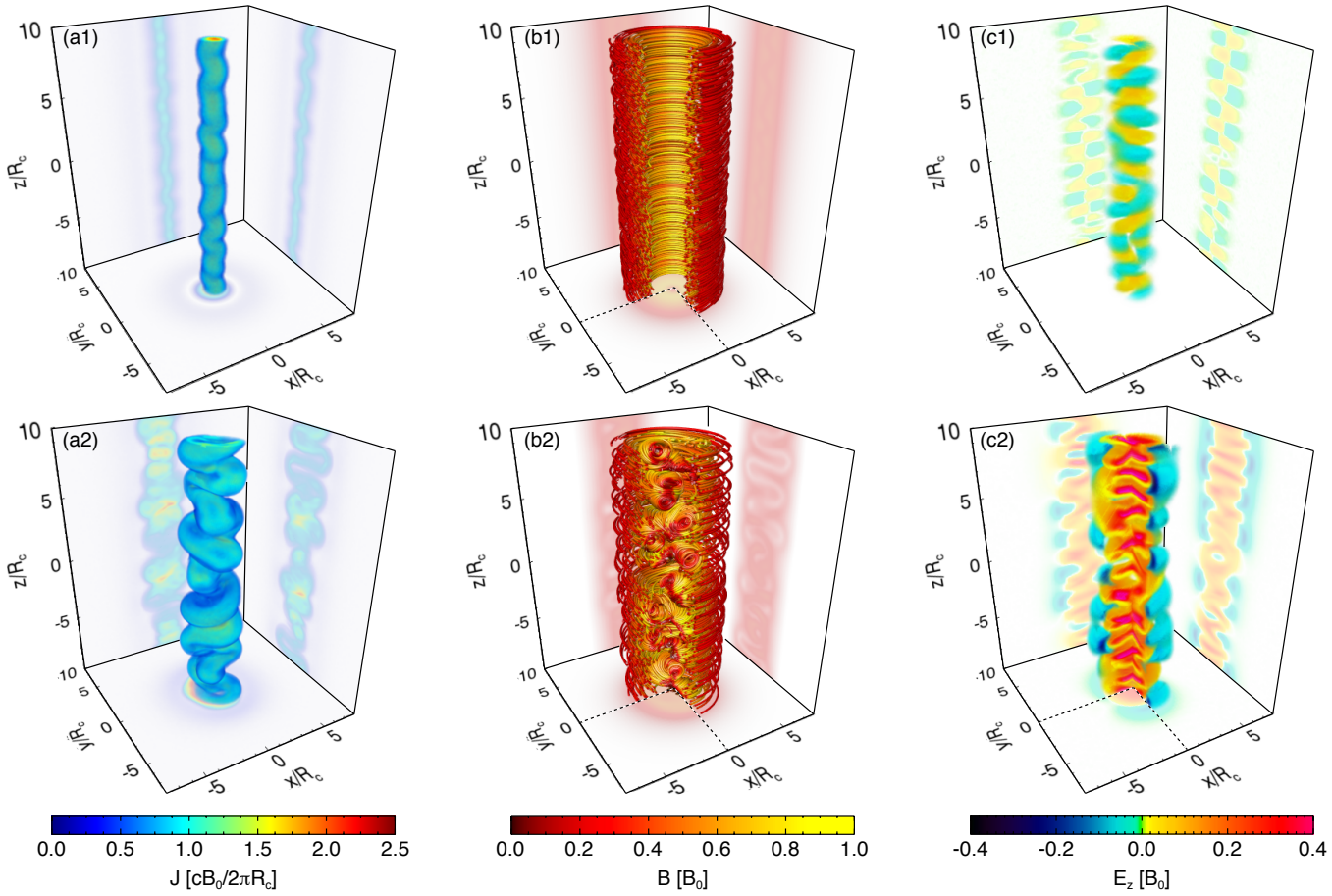

FIG. 1. Evolution of the jet structure subject to the kink instability. (a) Current density, (b) magnetic field lines, and (c) axial electric field, taken at times 1) $ct/R_c = 16$ and 2) $ct/R_c = 24$. These times correspond to the linear and nonlinear stages of the kink instability. Note that a quarter of the simulation box has been removed in (b1), (b2), and (c2) to reveal the inner field structure of the jet.

equilibrium; the net-inward magnetic stress is balanced by increased thermal pressure near the axis (see Supplemental Material [18]). This setup approximates the jet spine after the plasma has been focused towards the axis by recollimation, at the moment when it stagnates and is most vulnerable to the internal KI. We consider magnetic field profiles of the form $\mathbf{B}(r) = B_0 \frac{r}{R_c} e^{1-r/R_c} \mathbf{e}_\phi + B_z \mathbf{e}_z$, where R_c is the cross-sectional radius of the jet spine. We have also tested toroidal magnetic field profiles that decay as $r^{-\alpha}$ (with $\alpha \geq 1$), and determined that our overall findings are not sensitive to the structure of the magnetic field far from R_c. Near the black hole, the poloidal and toroidal magnetic field components (B_z and B_ϕ, respectively) are comparable to one another [19]. However, B_z/B_ϕ decreases with distance from the source, and can be very small at the relevant $\sim 100\,\mathrm{pc}$ distances. The characteristic magnetic field amplitude (henceforth denoted as B_0) at these distances, $B_0 \sim$ mG, is quite strong in the sense that the ratio σ of the magnetic to plasma rest-mass energy densities may exceed unity. The simulations cover values of $\sigma = 1-10$ and $B_z/B_\phi = 0.0-0.5$.

We utilize the fully kinetic electromagnetic PIC code OSIRIS 3.0 [20, 21]. Our simulations resolve a large dynamic range in 3D, enabling us to study the interplay between the evolution of the KI at large scales and the dynamics of particles at small scales, i.e. between the MHD physics of the jet spine at $\sim R_c$ and the kinetic physics operating at the particle gyroradius scale $\rho_g \ll R_c$. By systematically increasing the scale separation $\bar{R} \equiv R_c/\langle\rho_g\rangle$, we find asymptotic behavior in the particle acceleration physics as $\bar{R} \gg 1$. The dimensions of the simulated domains are $20 \times 20 \times (10-20)\ R_c^3$, with the jet located at the center of the domain and oriented along $\hat{\mathbf{z}}$. The simulations resolve the gyroradius of thermal particles at the core of the jet, $\langle\rho_g\rangle$, with $4-12$ points, and use $8-16$ particles per cell per species [18]. Our largest simulations attain $\bar{R} = 50$ and are state-of-the-art in computational scale, following 550 billion particles in $4096 \times 4096 \times 2048$ computational cells.

All of our simulations exhibit qualitatively similar dy-

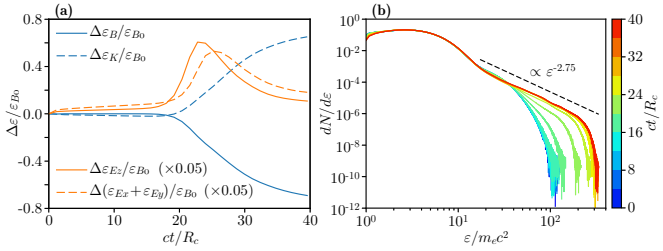

FIG. 2. (a) Temporal evolution of the magnetic, electric and particle kinetic energies integrated over the simulation domain. The left vertical axis refers to the variation of the magnetic ($\Delta\epsilon_B$) and particle kinetic ($\Delta\epsilon_K$) energies. The right vertical axis corresponds to the energy in the axial (ϵ_{Ez}) and transverse ($\epsilon_{Ex}+\epsilon_{Ey}$) components of the electric field. (b) Temporal evolution of the particle energy spectrum. The power-law tail extends beyond $\varepsilon_{\rm conf} = 125\ m_ec^2$.

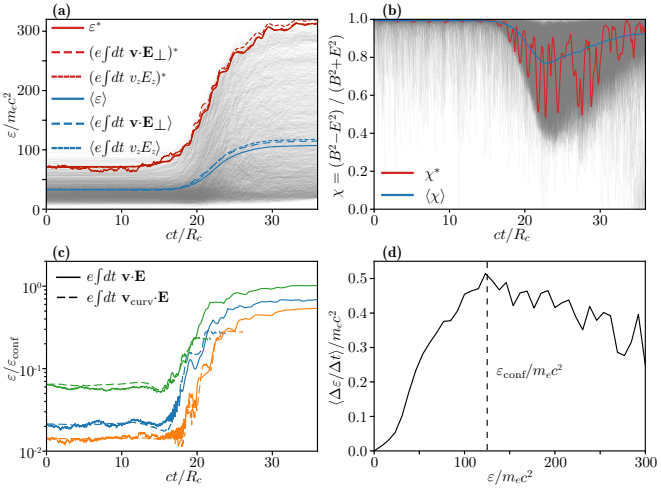

FIG. 3. (a) Evolution of particle energy ε and (b) relative magnitude of E and B experienced by a representative sample of 2000 nonthermal particles (grey curves). The red (blue) solid lines correspond to the highest (average) energy gain of the sample. The dashed and dotted curves indicate the integrated work done by $E_\perp$ and E_z, respectively, revealing that $E \simeq E_\perp \simeq E_z$ accounts for almost the entirety of the energy gain. (c) Evolution of the energy of 3 representative particles that start highly magnetized and reach $\varepsilon \sim \varepsilon_{\rm conf}$ (solid blue, orange, and green curves). Their acceleration is enabled by the curvature drift motion (dashed curves; these curves are interrupted when the guiding center description breaks down). (d) Mean energization rate, $\langle\Delta\varepsilon/\Delta t\rangle$, as a function of energy, ε, experienced by the 2000 nonthermal particles during the period $18 < ct/R_c < 30$. The vertical dashed line corresponds $\varepsilon_{\rm conf}$.

namics, illustrated in Figs. 1 and 2 for a jet with $\bar{R} \simeq 8$, $\sigma = 5$, and purely toroidal magnetic field ($B_z = 0$). The KI is triggered by thermal fluctuations in the plasma, and induces a growing helical modulation of the jet spine (top row of Fig. 1) with wavelength $\sim R_c$, consistent with linear theory and MHD simulations [22]. These transverse motions give rise to an inductive electric field, $\mathbf{E} = -\mathbf{v}\times\mathbf{B}$. At early times, the axial component of this electric field is harmonic, with zero net value along $\hat{\mathbf{z}}$, $\langle E_z\rangle \simeq 0$ [Fig. 1(c1)]. Notably, we observe that as the instability becomes nonlinear, and the transverse displacements of the jet become comparable to its radius, regions of like-oriented electric field are brought into alignment (Supplemental Fig. S1). This leads to the formation of a coherent inductive electric field throughout the spine region of the jet, with net value $\langle E_z\rangle \simeq 0.2B_0$ [Fig. 1(c2); a similar E_z field is observed in MHD simulations (not shown here) of the same configuration]. At the same time, strong distortions of the electrical current give rise to a highly tangled magnetic field structure, particularly in the central region where the coherent axial electric field has developed [Fig. 1(b2)]. This configuration of electric and magnetic fields facilitates rapid and efficient transfer of energy from the magnetic field to the plasma particles [Fig. 2(a)], with $\gtrsim 60\%$ of the magnetic energy being dissipated, and the overall plasma magnetization being reduced to $\sim 20\%$ of its initial value. This process is completed on a time scale $\tau_{\rm KI} \simeq 10R_c/c$, which is given by the transit time $2R_c/v_{\rm KI}$ of the KI-induced transverse motions across the jet diameter, with characteristic speed $v_{\rm KI} \simeq \langle E_z\rangle/B_0c \simeq 0.2c$.

The combination of electric and magnetic fields produced during the nonlinear stage of the KI is a potent accelerator of nonthermal particles. This is demonstrated by the formation of a nonthermal power-law tail in the particle energy spectrum, $dN/d\varepsilon \propto \varepsilon^{-p}$ with index $p = 2.75$ [Fig. 2(b)], that contains $\sim 50\%$ of the initial magnetic energy. Moreover, the nonthermal component of the spectrum extends to the confinement energy $\varepsilon_{\rm conf} \equiv eB_0R_c$, above which it rolls over as particles escape the system. The exceptional particles that attain the maximum energy do so by traveling along the jet axis $\hat{z}$ near the speed of light throughout the dynamical time of the KI; $\Delta\varepsilon_{\rm max} \simeq e\langle E_z\rangle c\tau_{\rm KI} \simeq 2eB_0R_c = 2\varepsilon_{\rm conf}$. We have found that the power-law index decreases for weaker magnetizations, becoming $p \simeq 2$ for $\sigma \simeq 1$ (Supplemental Fig. S2). This indicates that for $\sigma \simeq 1$, the highest energy particles can acquire a significant fraction of the jet's internal magnetic energy.

In order to uncover the mechanism responsible for the observed particle acceleration, we have performed a detailed analysis of the trajectories and the electromagnetic fields experienced by a representative sample of nonthermal particles [18]. Importantly, we find that these particles are primarily energized by the inductive electric field, $\mathbf{E} = -\mathbf{v}\times\mathbf{B} \simeq E_z\hat{\mathbf{z}}$, which implies $|\mathbf{E}| < |\mathbf{B}|$ [Fig. 3(a),(b)]. Nonideal, or parallel ($\mathbf{E} \parallel \mathbf{B}$) electric fields, commonly associated with the reconnection of magnetic field lines [23], are thus not responsible for the observed particle acceleration.

Acceleration by an inductive electric field $\mathbf{E} \perp \mathbf{B}$ re-

quires that particles cross magnetic field lines. This strongly suggests that magnetic field inhomogeneities must be crucial in the acceleration process. Indeed, our simulations reveal that the magnetic field becomes highly tangled, developing a spectrum of fluctuations over the complete range of scales, from R_c down to the gyroradius scale $\langle\rho_g\rangle$ of thermal particles (Supplemental Fig. S3). We find that these fluctuations enable rapid displacement of particles across magnetic field lines via the guiding center curvature drift with velocity $\mathbf{v}_{\rm curv} = \gamma m v_\parallel^2 c\, \mathbf{B}\times\boldsymbol{\kappa}/eB^2$ [24] [Fig. (3c)]; $v_\parallel$ is the particle velocity parallel to the local magnetic field and $\boldsymbol{\kappa}\equiv \mathbf{B}\cdot\nabla\mathbf{B}/B^2$ is the magnetic field curvature vector. These drifts allow particles to gain energy from the inductive electric field, with the instantaneous rate of energy gain being connected to the spatial and temporal distribution of the magnetic field curvature. Fig. 3(c) illustrates the energy evolution of particles that start highly magnetized and reach the confinement energy. These particles experience fast energy gains by encountering regions where the field curvature radius κ^{-1} is only a few times their gyroradius. Once they are accelerated to a large fraction $(0.2-0.3)$ of the confinement energy, the guiding center approximation breaks down [Fig. (3c)], and particles become effectively unmagnetized, moving with $v_z\sim c$ along the jet axis. The acceleration stops when the particles either escape the jet spine in the transverse direction or when the electric field decays as the instability subsides.

The mean energization rate $\langle\Delta\varepsilon/\Delta t\rangle$ increases with ε until $\varepsilon\lesssim\varepsilon_{\rm conf}$ [Fig. 3(d)], indicating a first-order Fermi process. This is consistent with acceleration via the curvature drift (since $v_{\rm curv}\propto\gamma$), the importance of which has also been identified in simulations of reconnecting current layers [25, 26]. We have confirmed that the same acceleration physics takes place in simulations with nonzero poloidal magnetic field, $B_z\lesssim 0.5B_\phi$, yielding similar power-law particle energy spectra as the purely toroidal field case (Supplemental Fig. S4).

The acceleration mechanism unveiled here is thus a consequence of a large-scale ($\sim R_c$) inductive electric field acting in concert with a magnetic field that is tangled over a range of scales that extends down to $\langle\rho_g\rangle$. These conditions are intrinsically 3D and arise self-consistently via the dynamic evolution of the KI [18]. While the scales of R_c and ρ_g are vastly disparate in astrophysical jets, a small fraction of the initially thermal particles can always attain the confinement energy $\varepsilon_{\rm conf}$. We have confirmed this by systematically increasing the ratio $\bar{R}$ of the jet radius to the gyroradius of the thermal particles. The power-law spectral index is preserved, consistently extending from the thermal mean up to $\varepsilon_{\rm conf}$, and the maximum particle energy gain is always $\Delta\varepsilon_{\rm max}\simeq 2eB_0R_c$ (Fig. 4). This indicates that our results may be extrapolated to astrophysical systems, where the enormous scale separation implies huge energy gains.

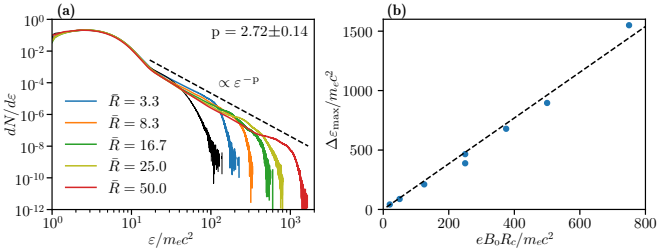

FIG. 4. (a) Final particle spectra for different system sizes ($\bar{R}$) and fixed magnetization $\sigma=5$. The black curve corresponds to initial particle spectrum, which is the same for all system sizes. (b) Scaling law of maximum particle energy gain with system size and magnetic field magnitude. The dots represent the results of 3D PIC simulations for different σ and $\bar{R}$, and the dashed line represents the linear fit $\Delta\varepsilon_{\rm max}m_ec^2\simeq 1.9\,\varepsilon_{\rm conf}=1.9\,eB_0R_c$.

Particle acceleration enabled by the KI can account for the synchrotron and inverse Compton (IC) radiating electrons in AGN jets. For example, the synchrotron energy spectrum, $F_\nu\propto\nu^{-\alpha}$, of knots such as HST-1 in M87 extends to hard X-rays, with spectral index $\alpha\simeq 1.0-1.5$ [5, 27]. The balance between synchrotron cooling and electron acceleration by the KI will steepen the electron spectrum, such that α is related to the spectral index p of the injected particles by $\alpha=p/2$ [18]. This is in agreement with our results that show $p=2-3$ for magnetization levels $\sigma=1-10$ (Supplemental Fig. S2). The same population of relativistic electrons produces IC radiation at GeV - TeV photon energies, by up-scattering its own synchrotron (or ambient) photons [28].

Protons and heavier ions are accelerated in the kink-unstable region of AGN jets in a similarly efficient way. This has been confirmed in simulations (Supplemental Fig. S5) with plasma having 1 proton per 10 electrons, the composition that is inferred by calorimetric modeling of many giant radio lobes [29]. Unlike electrons, proton synchrotron losses are negligible up to and beyond the confinement energy. In HST-1, whose intrinsic scale is $R_c\sim$ pc and magnetic field is $B_0\sim 1-10$ mG, protons could attain energies $10^{18}-10^{19}$ eV by residing in the accelerating region throughout the $\tau_{KI}\sim 30$ yr (comoving) dynamical time of KI. The brightest feature of M87, Knot A [30], has a significantly larger intrinsic scale $R_c\sim 100$ pc and may also possess mG-level magnetic fields. Under such conditions, the mechanism uncovered in this work would accelerate protons and iron nuclei to energies $\sim 10^{20}$ eV and $\sim 10^{21}$ eV respectively, with these most energetic particles acquiring a significant fraction of the jet's internal energy.

In summary, we have uncovered an efficient and robust particle acceleration mechanism that operates on the helical magnetic field structure of relativistic jets. It has long been appreciated [31] that in AGN jets, $\varepsilon_{\rm conf}$ may

exceed 10^{20} eV, which has made them prime UHECR source candidates. We have shown that charged particles can be efficiently accelerated to this limiting energy as a consequence of the internal KI, thus revealing a specific mechanism by which AGN jets could accelerate UHECRs. Our work also sheds new light on the generation of high-energy radiating particles in astrophysical jets and on the dependence of the radiation spectral index on the jet magnetization. We note that this mechanism can operate similarly in other astrophysical environments. Important examples are the Crab and other pulsar wind nebulae, for which the formation of a kink-unstable plasma column at high latitudes is observed and is expected to be a primary site where the pulsar's magnetic energy is dissipated [32–35].

The authors thank G. Madejski and R. Blandford for helpful discussions. This work was supported by the U.S. Department of Energy SLAC Contract No. DE-AC02-76SF00515, by the U.S. DOE Office of Science, Fusion Energy Sciences under FWP 100237, and by the U.S. DOE Early Career Research Program under FWP 100331. The authors acknowledge the OSIRIS Consortium, consisting of UCLA and IST (Portugal) for the use of the OSIRIS 3.0 framework and the visXD framework. Simulations were run on Mira (ALCF) through an ALCC award.

* epalves@slac.stanford.edu
† fiuza@slac.stanford.edu

[1] A. Celotti and G. Ghisellini, Monthly Notices of the Royal Astronomical Society **385**, 283 (2008).
[2] M. Nagano and A. A. Watson, Reviews of Modern Physics **72**, 689 (2000).
[3] The Pierre Auger Collaboration, Science **318**, 938 (2007).
[4] The IceCube Collaboration et al., Science **361**, eaat1378 (2018).
[5] D. E. Harris, J. A. Biretta, W. Junor, E. S. Perlman, W. B. Sparks, and A. S. Wilson, The Astrophysical Journal **586**, L41 (2003).
[6] L. Stawarz, F. Aharonian, J. Kataoka, M. Ostrowski, A. Siemiginowska, and M. Sikora, Monthly Notices of the Royal Astronomical Society **370**, 981 (2006).
[7] O. Bromberg and A. Levinson, The Astrophysical Journal **699**, 1274 (2009).
[8] A. R. Bell, Monthly Notices of the Royal Astronomical Society **182**, 147 (1978).
[9] R. Blandford and D. Eichler, Physics Reports **154**, 1 (1987).
[10] L. Sironi, A. Spitkovsky, and J. Arons, The Astrophysical Journal **771**, 54 (2013).
[11] A. R. Bell, A. T. Araudo, J. H. Matthews, and K. M. Blundell, Monthly Notices of the Royal Astronomical Society **473**, 2364 (2018).
[12] M. C. Begelman, The Astrophysical Journal **493**, 291 (1998).
[13] D. Giannios and H. C. Spruit, Astronomy & Astrophysics **450**, 887 (2006).
[14] A. Tchekhovskoy and O. Bromberg, Monthly Notices of the Royal Astronomical Society: Letters **461**, L46 (2016).
[15] O. Bromberg and A. Tchekhovskoy, Monthly Notices of the Royal Astronomical Society **456**, 1739 (2016).
[16] R. B. Duran, A. Tchekhovskoy, and D. Giannios, Monthly Notices of the Royal Astronomical Society **469**, 4957 (2016).
[17] O. Porth and S. S. Komissarov, Monthly Notices of the Royal Astronomical Society **452**, 1089 (2015).
[18] See Supplemental Material [url] for more details, which includes Refs. [36-39].
[19] R. D. Blandford and R. L. Znajek, Monthly Notices of the Royal Astronomical Society **179**, 433 (1977).
[20] R. A. Fonseca, L. O. Silva, F. S. Tsung, V. K. Decyk, W. Lu, C. Ren, W. B. Mori, S. Deng, S. Lee, T. Katsouleas, and J. C. Adam, Computational Science-ICCS 2002, Pt III, Proceedings **2331**, 342 (2002).
[21] R. A. Fonseca, S. F. Martins, L. O. Silva, J. W. Tonge, F. S. Tsung, and W. B. Mori, Plasma Physics and Controlled Fusion **50**, 124034 (2008).
[22] Y. Mizuno, Y. Lyubarsky, K.-I. Nishikawa, and P. E. Hardee, The Astrophysical Journal **728**, 90 (2011).
[23] L. Sironi and A. Spitkovsky, The Astrophysical Journal **783**, L21 (2014).
[24] T. G. Northrop, Reviews of Geophysics **1**, 283 (1963).
[25] J. T. Dahlin, J. F. Drake, and M. Swisdak, Physics of Plasmas **21**, 092304 (2014).
[26] F. Guo, X. Li, H. Li, W. Daughton, B. Zhang, N. Lloyd-Ronning, Y.-H. Liu, H. Zhang, and W. Deng, The Astrophysical Journal **818**, L9 (2016).
[27] D. E. Harris and H. Krawczynski, Annual Review of Astronomy and Astrophysics **44**, 463 (2006).
[28] W. J. Potter and G. Cotter, Monthly Notices of the Royal Astronomical Society **423**, 756 (2012).
[29] P. Pjanka, A. A. Zdziarski, and M. Sikora, Monthly Notices of the Royal Astronomical Society **465**, 3506 (2016).
[30] L. Stawarz, A. Siemiginowska, M. Ostrowski, and M. Sikora, The Astrophysical Journal **626**, 120 (2005).
[31] A. M. Hillas, Annual Review of Astronomy and Astrophysics **22**, 425 (1984).
[32] M. C. Begelman and Z.-Y. Li, The Astrophysical Journal **426**, 269 (1994).
[33] Y. E. Lyubarsky, Monthly Notices of the Royal Astronomical Society **427**, 1497 (2012).
[34] O. Porth, S. S. Komissarov, and R. Keppens, Monthly Notices of the Royal Astronomical Society **438**, 278 (2013).
[35] J. Zrake and J. Arons, The Astrophysical Journal **847**, 57 (2017).
[36] Y. Lyubarsky, The Astrophysical Journal **698**, 1570 (2009).
[37] G. Bateman, *Cambridge, Mass., MIT Press, 1978. 270 p.* (1978).
[38] S. Zenitani and M. Hoshino, The Astrophysical Journal **618**, L111 (2005).
[39] J. R. Jokipii, J. Kota, and J. Giacalone, Geophysical Research Letters (ISSN 0094-8276) **20**, 1759 (1993).